Partially coherent isodiffracting pulsed beams

Matias Koivurova,[1,*] Chaoliang Ding,[2] Jari Turunen,[1] and Liuzhan Pan[2]
[1]*University of Eastern Finland, Institute of Photonics, P. O. Box 111, FI-80101 Joensuu, Finland*
[2]*Department of Physics and Henan Key Laboratory of Electromagnetic Transformation and Detection, Luoyang Normal University, Luoyang 471934, China*

(Received 28 December 2017; published 14 February 2018)

We investigate a class of isodiffracting pulsed beams, which are superpositions of transverse modes supported by spherical-mirror laser resonators. By employing modal weights that, for stationary light, produce a Gaussian Schell-model beam, we extend this standard model to pulsed beams. We first construct the two-frequency cross-spectral density function that characterizes the spatial coherence in the space-frequency domain. By assuming a power-exponential spectral profile, we then employ the generalized Wiener-Khintchine theorem for nonstationary light to derive the two-time mutual coherence function that describes the space-time coherence of the ensuing beams. The isodiffracting nature of the laser resonator modes permits all (paraxial-domain) calculations at any propagation distance to be performed analytically. Significant spatiotemporal coupling is revealed in subcycle, single-cycle, and few-cycle domains, where the partial spatial coherence also leads to reduced temporal coherence even though full spectral coherence is assumed.

DOI: 10.1103/PhysRevA.97.023825

I. INTRODUCTION

One of the well-known properties of spherical-mirror laser cavities is that the spatial scale of the transverse cavity modes depends on the frequency ω (or wavelength λ) of the radiation [1]. In continuous-wave lasers the small spectral bandwidth implies that this dependence is negligible, and the same applies to pulsed lasers in the many-cycle regime. However, advances in mode locking of lasers open prospects for generating single-cycle pulses even in the visible region [2–4]. Pulses in this regime have such large spectral bandwidths that the frequency dependence of the modal scale must be considered; coherent (single-spatial-mode) subcycle, single-cycle, and few-cycle optical pulses are known to feature strong spatiotemporal coupling effects [5–7].

If more than one transverse mode is supported by a laser cavity, the emitted radiation becomes spatially partially coherent [8]. The most commonly used model for stationary partially coherent beams is the Gaussian Schell model (GSM) [9], which results from superpositions of Hermite-Gaussian (HG) laser cavity modes that satisfy a certain power-law weight distribution at a given frequency [10,11]. There are several studies on the extension of the GSM to pulsed beams [12–18]. However, in all of these studies the source field is described by frequency-independent transverse scale parameters, and hence the resulting models are not applicable to pulses with time scales of few cycles or less. Fundamental problems emerge with extensions of the GSM to ultrashort pulses if a Gaussian spectral distribution is associated with the field (as has been customary). These problems arise from the negative frequency components in the spectrum (unless they are truncated), and they do not vanish even if the contribution of the negative components is very small [6].

In the present paper we extend the GSM for stationary (polychromatic) beams to pulsed beams by making use of the coherence theory of nonstationary fields [19,20]. We assume that the spatial modes are of the usual HG form and have the frequency-dependent transverse scaling that follows from the theory of spherical-mirror laser resonators. The modal weights are chosen to obey the same power-law distribution that leads to stationary GSM beams. Furthermore, in describing the space-time properties of the pulsed fields, we use a power-exponential spectral distribution that does not contain negative frequencies.

In Sec. II we consider polychromatic stationary GSM beams [21], which satisfy the correct spectral scaling law of the HG modes. This model is extended in Sec. III to partially coherent pulsed beams in the space-frequency domain, where our pulses share the isodiffracting character of stationary GSM beams: shape-invariant propagation with a monotonously increasing transverse scale at each single frequency. In Sec. IV we introduce the power-exponential spectral distribution and derive the space-time characteristics of the pulsed beams by evaluating the two-time mutual coherence function in terms of Gauss hypergeometric functions. The main space-time properties of our model pulses, including spatiotemporal coupling and the reduction of temporal coherence due to partial spatial coherence, are illustrated in Sec. V. Final remarks and conclusions are provided in Sec. VI.

II. STATIONARY ISODIFFRACTING BEAMS

Let us start from the coherent-mode representation of stationary GSM beams [10,11], which is a weighted superposition of HG modes. Since these modes are separable in cartesian coordinates, it is sufficient to consider one-dimensional representations in, say, x direction.

The waist of a HG mode of order m originating from a stable laser cavity has a space-frequency representation of the

*matias.koivurova@uef.fi

form [1]

$$\psi_m(x;\omega) = g(\omega)\frac{(2/\pi)^{1/4}}{\sqrt{2^m m! w_0(\omega)}} \times H_m\left[\frac{\sqrt{2}x}{w_0(\omega)}\right]\exp\left[-\frac{x^2}{w_0^2(\omega)}\right], \quad (1)$$

where H_m is a Hermite polynomial of order m. The spatial beam width at the waist varies with ω as

$$w_0(\omega) = \sqrt{\frac{\omega_0}{\omega}}w_0. \quad (2)$$

Here $w_0 = w(\omega_0)$ is the beam width at reference frequency ω_0, which may be chosen as the peak or mean frequency of the (possibly complex-valued) spectral weight function $g(\omega)$. This function can be chosen to fulfill the normalization condition $\int |g(\omega)|^2 d\omega = 1$, but we consider a more general case where the integral $\int |g(\omega)|^2 d\omega$ yields an arbitrary but finite constant. By assuming that $g(\omega)$ is the same for all m we neglect the small differences in the resonance frequencies of the transverse modes [1]. This assumption is well justified for the short pulses considered below, since the spectral width of $g(\omega)$ is then far greater than the modal frequency separation.

The space-frequency-domain coherence properties of steady-state (stationary) fields are characterized by the cross-spectral density (CSD) function. If more than one mode is present in a stationary field, any incoherent superposition of the type [22]

$$W(x_1,x_2;\omega) = \sum_{m=0}^{\infty} c_m(\omega)\psi_m^*(x_1;\omega)\psi_m(x_2;\omega) \quad (3)$$

represents a valid CSD. In particular, we may choose the weights $c_m(\omega)$ as [10,11,23]

$$c_m = w_0\sqrt{\frac{2\pi}{\beta}}\frac{1}{1+1/\beta}\left(\frac{1-\beta}{1+\beta}\right)^m, \quad (4)$$

where we have assumed them to be independent on ω (though in general needs not be the case). In Eq. (4), β is a parameter that can vary in the range $0 \leqslant \beta \leqslant 1$, where the lower and upper bounds represent full incoherence and full coherence, respectively. The effective (or overall) degree of spatial coherence of the field [24] now has the form

$$\bar{\mu} = \frac{\left[\sum_{m=0}^{\infty} c_m^2\right]^{1/2}}{\sum_{m=0}^{\infty} c_m} = \sqrt{\beta}, \quad (5)$$

thus being simply related to the parameter β.

On inserting from Eqs. (1), (2), and (4) into Eq. (3) and rearranging the terms we get

$$W(x_1,x_2;\omega) = \frac{2}{\sqrt{\beta}}\frac{1}{1+1/\beta}\sqrt{\frac{\omega}{\omega_0}}|g(\omega)|^2 \times \exp\left(-\frac{\omega}{\omega_0}\frac{x_1^2+x_2^2}{w_0^2}\right)\sum_{m=0}^{\infty} H_m\left(\sqrt{\frac{\omega}{\omega_0}}\frac{\sqrt{2}x_1}{w_0}\right) \times H_m\left(\sqrt{\frac{\omega}{\omega_0}}\frac{\sqrt{2}x_2}{w_0}\right)\frac{t^m}{m!}, \quad (6)$$

where

$$t = \frac{1}{2}\frac{1-\beta}{1+\beta}. \quad (7)$$

We immediately recognize that Eq. (6) is an exponential generating function of the form

$$\sum_{m=0}^{\infty} H_m(x)H_m(y)\frac{t^m}{m!} = \frac{1}{\sqrt{1-4t^2}}\exp\left[-\frac{4t^2(x^2+y^2)-4xyt}{1-4t^2}\right], \quad (8)$$

where the equality is valid when $|t| \neq 1/2$ (for $|t| = 1/2$ the summation leads to the Dirac delta function). On substituting from Eq. (8) to Eq. (6) and simplifying, we obtain

$$W(x_1,x_2;\omega) = \sqrt{\frac{\omega}{\omega_0}}|g(\omega)|^2\exp\left(-\frac{1+\beta^2}{2\beta}\frac{\omega}{\omega_0}\frac{x_1^2+x_2^2}{w_0^2}\right) \times \exp\left(\frac{1-\beta^2}{\beta}\frac{\omega}{\omega_0}\frac{x_1x_2}{w_0^2}\right). \quad (9)$$

We can, in general, express the CSD in terms of the spectral density $S(x;\omega) = W(x,x;\omega)$ and the complex spectral degree of spatial coherence $\mu(x_1,x_2;\omega)$ as

$$W(x_1,x_2;\omega) = [S(x_1;\omega)S(x_2;\omega)]^{1/2}\mu(x_1,x_2;\omega). \quad (10)$$

It then follows from Eq. (9) that the spectral density has the Gaussian form

$$S(x;\omega) = \sqrt{\frac{\omega}{\omega_0}}|g(\omega)|^2\exp\left(-\frac{\omega}{\omega_0}\frac{2x^2}{w^2}\right), \quad (11)$$

where

$$w = \frac{w_0}{\sqrt{\beta}}. \quad (12)$$

The spectral degree of spatial coherence is also a Gaussian function

$$\mu(x_1,x_2;\omega) = \exp\left[-\frac{\omega}{\omega_0}\frac{(x_1-x_2)^2}{2\sigma^2}\right], \quad (13)$$

where the parameter

$$\sigma = \frac{\beta}{\sqrt{1-\beta^2}}w = \frac{\sqrt{\beta}}{\sqrt{1-\beta^2}}w_0 \quad (14)$$

describes the spatial coherence width of the field at the plane of the waist for $\omega = \omega_0$. Full spatial coherence and incoherence are obtained in the limits $\sigma \to \infty$ and $\sigma \to 0$, respectively.

The expressions given above describe the waist of a stationary isodiffracting Gaussian Schell-model beam; the term Schell model refers to the fact $\mu(x_1,x_2;\omega)$ is a function of the spatial coordinate difference $\Delta x = x_2 - x_1$ only. Since Eq. (14) leads to the relation

$$\beta = \left(1+\frac{w^2}{\sigma^2}\right)^{-1/2}, \quad (15)$$

the coherent and incoherent limits defined in terms of σ agree with the one defined above in terms of β. Moreover, β and Eq. (12) determine the scale w_0 of the coherent modes in Eq. (1), if the coherence width σ and the beam width w at the plane of the waist have been fixed. Considering an arbitrary

frequency, the coherence width is $\sigma(\omega) = \sigma\sqrt{\omega_0/\omega}$ and the beam width is $w(\omega) = w\sqrt{\omega_0/\omega}$. Hence the ratio

$$\frac{\sigma(\omega)}{w(\omega)} = \frac{\sigma}{w} \tag{16}$$

is independent on ω. This may be considered as a characteristic property of stationary, isodiffracting GSM beams generated in spherical-mirror cavities.

III. PULSES IN SPACE-FREQUENCY DOMAIN

If more than one spatial mode is present in a nonstationary field, but each mode is spectrally fully coherent, the two-frequency CSD may then be expressed in the form of a coherent-mode superposition [14]

$$W(x_1,x_2;\omega_1,\omega_2) = \sum_{m=0}^{\infty} c_m \psi_m^*(x_1;\omega_1)\psi_m(x_2;\omega_2), \tag{17}$$

where the coefficients c_m must be independent on the frequencies ω_1 and ω_2. The effective degree of spatial coherence is still given by Eq. (5), which is valid in both space-frequency and space-time domains [14], independently on the choice of $g(\omega)$.

On inserting from Eqs. (1), (2), and (4) into Eq. (17) we have

$$\begin{aligned} W(x_1,x_2;\omega_1,\omega_2) = {} & \frac{2}{\sqrt{\beta}}\frac{1}{1+1/\beta}\left(\frac{\omega_1}{\omega_0}\frac{\omega_2}{\omega_0}\right)^{1/4} \\ & \times g^*(\omega_1)g(\omega_2)\exp\left(-\frac{\omega_1 x_1^2+\omega_2 x_2^2}{\omega_0 w_0^2}\right) \\ & \times \sum_{m=0}^{\infty} H_m\left(\sqrt{\frac{\omega_1}{\omega_0}}\frac{\sqrt{2}x_1}{w_0}\right) \\ & \times H_m\left(\sqrt{\frac{\omega_2}{\omega_0}}\frac{\sqrt{2}x_2}{w_0}\right)\frac{t^m}{m!}, \end{aligned} \tag{18}$$

where t is again given by Eq. (7). Using Eq. (8) we now obtain

$$\begin{aligned} W(x_1,x_2;\omega_1,\omega_2) = {} & \left(\frac{\omega_1}{\omega_0}\frac{\omega_2}{\omega_0}\right)^{1/4} g^*(\omega_1)g(\omega_2) \\ & \times \exp\left(-\frac{1+\beta^2}{2\beta}\frac{\omega_1 x_1^2+\omega_2 x_2^2}{\omega_0 w_0^2}\right) \\ & \times \exp\left(\frac{1-\beta^2}{\beta}\frac{\sqrt{\omega_1\omega_2}}{\omega_0}\frac{x_1 x_2}{w_0^2}\right). \end{aligned} \tag{19}$$

Representing the two-frequency CSD in terms of the spectral density and the two-frequency complex degree of spatial coherence as

$$W(x_1,x_2;\omega_1,\omega_2) = [S(x_1;\omega_1)S(x_2;\omega_2)]^{1/2}\mu(x_1,x_2;\omega_1,\omega_2), \tag{20}$$

we find that the spectral density has exactly the same form as in the stationary case in Eq. (11). Furthermore, the complex degree of spatial coherence can be cast in the form

$$\begin{aligned} \mu(x_1,x_2;\omega_1,\omega_2) = {} & \exp\left[-\frac{\left(\sqrt{\omega_1}x_1-\sqrt{\omega_2}x_2\right)^2}{2\omega_0\sigma^2}\right] \\ & \times \exp[i\varphi(\omega_1,\omega_2)], \end{aligned} \tag{21}$$

where σ is given by Eq. (14) and the phase

$$\varphi(\omega_1,\omega_2) = \arg[g(\omega_2)] - \arg[g(\omega_1)] \tag{22}$$

vanishes for real-valued spectral distributions $g(\omega)$.

When evaluated at a single frequency ($\omega_1 = \omega_2 = \omega$), this result reduces to Eq. (13). The model presented in this section can indeed be considered as an extension of an isodiffracting Gaussian Schell-model beam to the nonstationary case. It should be noted, however, that the field is not of the Schell-model form when two different frequencies are considered.

Let us consider paraxial free-space propagation of pulsed beams radiated by sources defined above. The propagated form of a HG mode of order m at distance z from the waist is [1]

$$\begin{aligned} \psi_m(x,z;\omega) = {} & g(\omega)\frac{(2/\pi)^{1/4}\exp[i\phi(z;\omega)]}{\sqrt{2^m m! w_0(z;\omega)}} H_m\left[\frac{\sqrt{2}x}{w_0(z;\omega)}\right] \\ & \times \exp\left[-\frac{x^2}{w_0^2(z;\omega)}\right]\exp\left[i\frac{\omega}{c}\frac{x^2}{2R(z)}\right], \end{aligned} \tag{23}$$

where c is the speed of light and the quantities

$$w_0(z;\omega) = \sqrt{\frac{\omega_0}{\omega}}w_0(z), \tag{24}$$

$$w_0(z) = w_0\left(1+\frac{z^2}{z_{\mathrm{R}}^2}\right)^{1/2}, \tag{25}$$

$$R(z) = z + \frac{z_{\mathrm{R}}^2}{z}, \tag{26}$$

$$\phi(z;\omega) = \frac{\omega}{c}z - \left(m+\frac{1}{2}\right)\arctan\left(\frac{z}{z_{\mathrm{R}}}\right), \tag{27}$$

$$z_{\mathrm{R}} = \frac{\omega w_0^2(\omega)}{2c} = \frac{\omega_0 w_0^2}{2c} \tag{28}$$

are the usual Gaussian-beam propagation parameters. The special feature of isodiffracting HG fields, which may be taken as their defining property, is that because the waist of the beam is frequency dependent, the Rayleigh range z_{R} is independent on the frequency.

Since the modes in Eq. (17) are mutually uncorrelated at the plane of the waist, they propagate independently of each other. Hence the CSD at any plane $z = \text{const}$, may be expressed as

$$W(x_1,x_2,z;\omega_1,\omega_2) = \sum_{m=0}^{\infty} c_m \psi_m^*(x_1,z;\omega_1)\psi_m(x_2,z;\omega_2), \tag{29}$$

where the coefficients c_m are the same as at the plane $z = 0$. Inserting from Eqs. (4), (23), and (24) into Eq. (29)

we obtain

$$W(x_1,x_2,z;\omega_1,\omega_2) = \frac{2}{\sqrt{\beta}}\frac{1}{1+1/\beta}\left(\frac{\omega_1}{\omega_0}\frac{\omega_2}{\omega_0}\right)^{1/4} \times g^*(\omega_1)g(\omega_2)\frac{w_0}{w_0(z)}\exp[-i(\omega_1-\omega_2)z/c] \times \exp\left(-\frac{\omega_1 x_1^2+\omega_2 x_2^2}{\omega_0 w_0^2(z)}\right)\exp\left[-\frac{i\left(\omega_1 x_1^2-\omega_2 x_2^2\right)}{2cR(z)}\right] \times \sum_{m=0}^{\infty} H_m\left(\sqrt{\frac{\omega_1}{\omega_0}}\frac{\sqrt{2}x_1}{w_0(z)}\right)H_m\left(\sqrt{\frac{\omega_2}{\omega_0}}\frac{\sqrt{2}x_2}{w_0(z)}\right)\frac{t^m}{m!}, \quad (30)$$

with t defined in Eq. (7). Using again Eq. (8), we have

$$W(x_1,x_2,z;\omega_1,\omega_2) = [S(x_1,z;\omega_1)S(x_2,z;\omega_2)]^{1/2}\mu(x_1,x_2,z;\omega_1,\omega_2), \quad (31)$$

where

$$S(x,z;\omega) = \sqrt{\frac{\omega}{\omega_0}}|g(\omega)|^2\frac{w}{w(z)}\exp\left[-\frac{\omega}{\omega_0}\frac{2x^2}{w^2(z)}\right], \quad (32)$$

with

$$w(z) = w\left(1+\frac{z^2}{z_R^2}\right)^{1/2} = \frac{w_0(z)}{\sqrt{\beta}} \quad (33)$$

and

$$|\mu(x_1,x_2,z;\omega_1,\omega_2)| = \exp\left[-\frac{(\sqrt{\omega_1}x_1-\sqrt{\omega_2}x_2)^2}{2\omega_0\sigma^2(z)}\right], \quad (34)$$

with

$$\sigma(z) = \frac{\sigma}{w}w(z). \quad (35)$$

Hence the ratio of the coherence width and the beam width (at any given frequency) remains constant upon propagation, as is the case for stationary Gaussian Schell-model beams. Finally, the phase of the complex degree of spatial coherence has the form

$$\arg[\mu(x_1,x_2,z;\omega_1,\omega_2)] = \arg[g(\omega_2)] - \arg[g(\omega_1)] - (\omega_1-\omega_2)z/c - \frac{\omega_1 x_1^2-\omega_2 x_2^2}{2cR(z)}, \quad (36)$$

where the most significant term is the last phase factor that represents a spherical wave with radius $R(z)$.

IV. PULSES IN SPACE-TIME DOMAIN

The space-time coherence properties of nonstationary fields are characterized by the two-time mutual coherence function (MCF) $\Gamma(x_1,x_2;t_1,t_2;z)$, which is connected to the CSD by the generalized Wiener-Khintchine theorem

$$\Gamma(x_1,x_2,z;t_1,t_2) = \iint_0^\infty W(x_1,x_2,z;\omega_1,\omega_2) \times \exp[i(\omega_1 t_1-\omega_2 t_2)]d\omega_1 d\omega_2. \quad (37)$$

The complex degree of coherence in the space-time domain is defined similarly to its spectral counterpart,

$$\gamma(x_1,x_2,z;t_1,t_2) = \frac{\Gamma(x_1,x_2,z;t_1,t_2)}{\sqrt{I(x_1,z;t_1)I(x_2,z;t_2)}}, \quad (38)$$

where $I(x,z;t) = \Gamma(x,x,z;t,t)$ is the spatiotemporal intensity distribution of the field. On inserting from Eqs. (31)–(36) into Eq. (37) we obtain

$$\Gamma(x_1,x_2,z;t_1,t_2) = \frac{w}{w(z)}\iint_0^\infty\left(\frac{\omega_1}{\omega_0}\frac{\omega_2}{\omega_0}\right)^{1/4} g^*(\omega_1)g(\omega_2)\exp\left[-\frac{\omega_1 x_1^2+\omega_2 x_2^2}{\omega_0 w^2(z)}\right]\exp\left[-\frac{\left(\sqrt{\omega_1}x_1-\sqrt{\omega_2}x_2\right)^2}{2\omega_0\sigma^2(z)}\right] \times \exp\left\{i\left[\omega_1 t_1-\omega_2 t_2-(\omega_1-\omega_2)\frac{z}{c}\right]\right\}\exp\left[-i\frac{\omega_1 x_1^2-\omega_2 x_2^2}{2cR(z)}\right]d\omega_1 d\omega_2. \quad (39)$$

This expression can be rearranged into the form

$$\Gamma(x_1,x_2,z;t_1,t_2) = \frac{w}{w(z)}\int_0^\infty\left(\frac{\omega_1}{\omega_0}\right)^{1/4} g^*(\omega_1)J(x_1,x_2,z;t_1,t_2,\omega_1)\exp\left[-T^*(x_1,z;t_1)\frac{\omega_1}{\omega_0}\right]d\omega_1, \quad (40)$$

where

$$T(x,z;t) = \left[\frac{1}{w^2(z)}+\frac{1}{2\sigma^2(z)}\right]x^2 + i\omega_0\left[t'-\frac{x^2}{2cR(z)}\right], \quad (41)$$

$t' = t - z/c$ is the retarded time, and

$$J(x_1,x_2,z;t_1,t_2,\omega_1) = \int_0^\infty\left(\frac{\omega_2}{\omega_0}\right)^{1/4} g(\omega_2)\exp\left[-T(x_2,z;t_2)\frac{\omega_2}{\omega_0}\right]\exp\left[\frac{x_1 x_2}{\sigma^2(z)}\sqrt{\frac{\omega_1}{\omega_0}}\sqrt{\frac{\omega_2}{\omega_0}}\right]d\omega_2. \quad (42)$$

To proceed further, we need to fix the spectral field distribution $g(\omega)$.

Let us assume that the spectral shape of the modes is of the power-exponential form (see, e.g., Ref. [25]) by writing

$$\left(\frac{\omega}{\omega_0}\right)^{1/4} g(\omega) = \frac{1}{\sqrt{\Gamma(2n)}}\left(2n\frac{\omega}{\omega_0}\right)^n\exp\left(-n\frac{\omega}{\omega_0}\right), \quad (43)$$

where n is a real and positive constant that can be varied to control the spectral bandwidth of the pulse train and $\Gamma(x)$ is the familiar gamma function. This expression is clearly not normalized, and it has its maximum at $\omega = \omega_0$, which is therefore a natural choice as the reference frequency. Another physically plausible wideband spectrum (with no negative frequencies) would be the blackbody spectrum considered in, e.g., Ref. [18]. However, the present choice leaves us far greater freedom to control the spectral bandwidth, which reduces as n increases. In fact, with large values of n, the spectral function in Eq. (43) approaches a Gaussian profile centered at $\omega = \omega_0$.

The final result for the spatiotemporal field is obtained by inserting from Eq. (43) into Eq. (42). The details of the derivation are presented in Appendix A. The final result can be conveniently represented as a sum of three terms:

$$\Gamma(x_1,x_2,z;t_1,t_2) = \sum_{j=1}^{3} \Gamma_j(x_1,x_2,z;t_1,t_2). \tag{44}$$

We will see below that these terms play an interesting role in characterization of spatiotemporal coupling. Explicitly, by denoting

$$T_n(x_1,x_2,z;t_1,t_2) = [T^*(x_1,z;t_1)+n][T(x_2,z;t_2)+n] \tag{45}$$

we have

$$\Gamma_1(x_1,x_2,z;t_1,t_2) = (2n)^{2n}\omega_0^2 \frac{\Gamma^2(n+1)}{\Gamma(2n)} \frac{w}{w(z)} T_n^{-(n+1)}(x_1,x_2,z;t_1,t_2)\, {}_2F_1\left[n+1,n+1;\frac{1}{2};\frac{x_1^2x_2^2}{4\sigma^4(z)T_n(x_1,x_2,z;t_1,t_2)}\right], \tag{46}$$

$$\Gamma_2(x_1,x_2,z;t_1,t_2) = -(2n)^{2n}\omega_0^2 \frac{\Gamma^2(n+3/2)}{(n+1)^2\Gamma(2n)} \frac{w}{w(z)} T_n^{-(n+3/2)}(x_1,x_2,z;t_1,t_2)\left[\frac{\sigma^2(z)}{x_1x_2}T_n(x_1,x_2,z;t_1,t_2) - \frac{x_1x_2}{4\sigma^2(z)}\right]$$
$$\times\, {}_2F_1\left[n+\frac{3}{2},n+\frac{3}{2};-\frac{1}{2};\frac{x_1^2x_2^2}{4\sigma^4(z)T_n(x_1,x_2,z;t_1,t_2)}\right], \tag{47}$$

$$\Gamma_3(x_1,x_2,z;t_1,t_2) = (2n)^{2n}\omega_0^2 \frac{\Gamma^2(n+3/2)}{(n+1)^2\Gamma(2n)} \frac{w}{w(z)} T_n^{-(n+3/2)}(x_1,x_2,z;t_1,t_2)\left[\frac{\sigma^2(z)}{x_1x_2}T_n(x_1,x_2,z;t_1,t_2) - \left(n+\frac{3}{2}\right)\frac{x_1x_2}{\sigma^2(z)}\right]$$
$$\times\, {}_2F_1\left[n+\frac{3}{2},n+\frac{3}{2};\frac{1}{2};\frac{x_1^2x_2^2}{4\sigma^4(z)T_n(x_1,x_2,z;t_1,t_2)}\right], \tag{48}$$

where ${}_2F_1(a,b;c;z)$ is the (Gauss) hypergeometric function.

Let us next consider the axial form of the temporal pulses by setting $x_1 = x_2 = 0$. All of the hypergeometric functions in the MCF then equal unity and $\Gamma_2 + \Gamma_3 = 0$. Now $T(0,z;t) = i\omega_0 t'$,

$$T_n(0,0,z;t_1,t_2) = n^2 + \omega_0^2 t_1' t_2' + in\omega_0\left(t_2' - t_1'\right), \tag{49}$$

with axial MCF taking the simple form

$$\Gamma(0,0,z;t_1,t_2) = (2n)^{2n}\omega_0^2 \frac{\Gamma^2(n+1)}{\Gamma(2n)} \frac{w}{w(z)}\left[n^2 + \omega_0^2 t_1' t_2' + in\omega_0(t_2' - t_1')\right]^{-(n+1)}. \tag{50}$$

The axial intensity is now given by

$$I(0,z;t) = (2n)^{2n}\omega_0^2 \frac{\Gamma^2(n+1)}{\Gamma(2n)} \frac{w}{w(z)}\left(n^2 + \omega_0^2 t'^2\right)^{-(n+1)} \tag{51}$$

and the on-axis complex degree of temporal coherence takes the form

$$\gamma(0,0,z;t_1,t_2) = \frac{\left[\left(n^2+\omega_0^2 t_1'^2\right)\left(n^2+\omega_0^2 t_2'^2\right)\right]^{(n+1)/2}}{\left[n^2 + \omega_0^2 t_1' t_2' + in\omega_0\left(t_2' - t_1'\right)\right]^{n+1}} \tag{52}$$

so that $|\gamma(0,0,z;t_1,t_2)| = 1$. Hence the axial field is temporally fully coherent for all values of w, σ, and n. The axial intensity distribution is a symmetric function of (retarded) time, with a full width at half-maximum

$$t'_{\mathrm{FWHM}} = T_0 \frac{n}{\pi}\sqrt{2^{1/(n+1)} - 1}, \tag{53}$$

where $T_0 = 2\pi/\omega_0$ is the duration of the optical cycle at frequency ω_0. Hence we are in the single-cycle regime when $n \sim 15$, clearly in the subcycle regime when $n < 10$, and in the few-cycle regime when $n \sim 50$ or larger. In the few-cycle regime the axial temporal intensity becomes nearly indistinguishable from a Gaussian profile with $1/e^2$ half-width $T = t'_{\mathrm{FWHM}}/\sqrt{2\ln 2}$.

On comparing the three contributions to the MCF in Eq. (44), we find that the terms Γ_2 and Γ_3 are a factor of $\sim(n+1)^{-2}$ smaller than Γ_1. Hence, when n is large, the dominant term is Γ_1. In the few-cycle regime the terms Γ_2 and Γ_3, which are mainly responsible for spatiotemporal coupling, can effectively be ignored.

V. ILLUSTRATIONS AND INTERPRETATIONS

Since the final result given by Eqs. (44)–(48) is not particularly transparent, we proceed to illustrate its main characteristics by plotting $\Gamma(x_1,x_2,z;t_1,t_2)$ as a function of selected parameters. It is convenient to use dimensionless quantities here: the transverse spatial coordinates x_1 and x_2 are

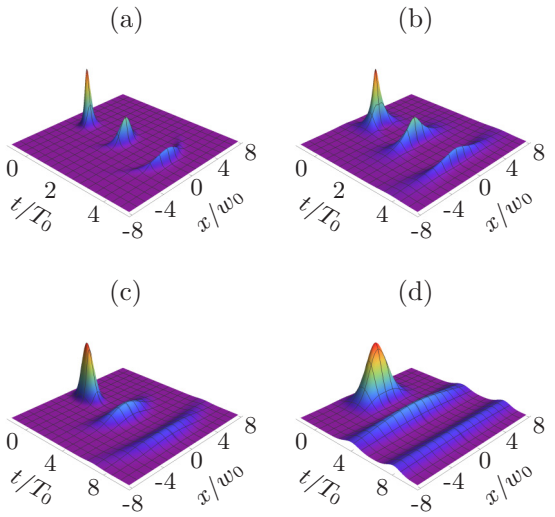

FIG. 1. Normalized spatiotemporal intensity profiles $I(x,z;t)$ at different propagation distances z. In the upper row $n = 1$ and pulses at distances $z/z_R = 0,2,4$ are shown for (a) $\beta = 1$ and (b) $\beta = 0.1$. In the lower row $n = 25$, $z/z_R = 0,4,8$, and pulses are shown for (c) $\beta = 1$ and (d) $\beta = 0.1$.

normalized to the modal scale parameter w_0, the longitudinal spatial coordinate z to the Rayleigh range z_R, and the temporal coordinates to T_0. The spectral width is controlled by varying the parameter n and the state of spatial coherence is controlled by the choice of β. Because of a numerical issue discussed in Appendix B, we consider pulses in the subcycle to few-cycle regimes (up to $n = 50$), where spatiotemporal coupling effects are most prominent.

In Fig. 1 we plot normalized spatiotemporal pulse intensity profiles $I(x,z;t)$ at different propagation distances. We consider both completely spatially coherent pulse trains with $\beta = 1$ (only mode $m = 0$ is present), and spatially partially coherent pulse trains with $\beta = 0.1$. The propagation distances are chosen to correspond to multiples $z_q = qz_R$ of the Rayleigh range z_R, and for clarity we show the pulses centered in the time domain at instants $t_q = qT_0$.

Several expected features are evident from Fig. 1. The pulses become temporally longer with increasing n, and spatially wider with decreasing β, as more and more modes with the same transverse scale factor w_0 emerge. The pulsed beam acquires a spherical-wave character upon propagation, as is usual for paraxial beam propagation. Strong spatiotemporal coupling is observed for $n = 1$, since the pulse profile at $z = 0$ features

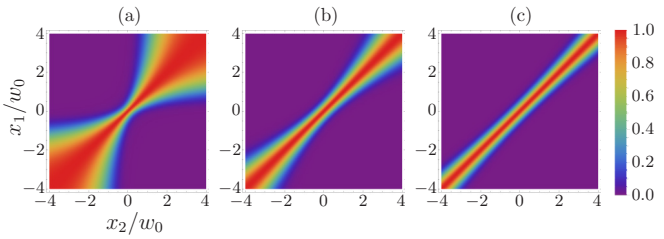

FIG. 3. Absolute value of complex degree of spatial coherence $|\gamma(x_1,x_2,0;0,0)|$ for $\beta = 0.1$. (a) Subcycle pulse with $n = 1$, (b) single-cycle pulse with $n = 10$, and (c) two-cycle pulse with $n = 50$.

spatial side lobes with temporal lengths much greater than the axial pulse duration. These effects are greatly reduced when $n = 25$—as expected—since the term Γ_1 becomes dominant. In this domain the temporal and spatial intensity distributions become nearly uncoupled. The temporal pulses approaches a Gaussian shape centered on a circle of radius $R(z)$, and the spatial intensity profiles approach Gaussian distributions as well, like in the case of stationary GSM beams.

Figure 2 illustrates the initial normalized spatiotemporal intensity profiles (at $z = 0$) in more detail. Here we consider pulses with a relatively low degree of spatial coherence ($\beta = 0.1$) and different spectral bandwidths. The spatiotemporal coupling effects reduce with increasing n and nearly vanish above the single-cycle regime.

Spatiotemporal coupling effects are also prominently present if we consider the coherence properties of ultrashort pulses. Figure 3 illustrates the absolute value of the time-domain complex degree of spatial coherence

$$\gamma(x_1,x_2,0;0,0) = \frac{\Gamma(x_1,x_2,0;0,0)}{\sqrt{I(x_1,0;0)I(x_2,0;0)}} \tag{54}$$

of the initial pulse ($z = 0$, $t_1 = t_2 = 0$). Obviously, for small values of n, the pulses do not obey the Schell model in the spatial domain since the distributions depend substantially on both x_1 and x_2, not only on their difference $\Delta x = x_2 - x_1$. The effective spatial coherence length (the width of the distribution in the antidiagonal direction) is shortest near the center of the pulse and increases with the average spatial coordinate $\bar{x} = \frac{1}{2}(x_1 + x_2)$. The effect is highly prominent for subcycle pulses, but diminishes rapidly in the few-cycle regime.

In view of Eq. (52), the field along the optical axis is fully temporally coherent regardless of the degree of spatial coherence or the bandwidth of the pulses. However, the off-axis degree of temporal coherence depends on both β and n.

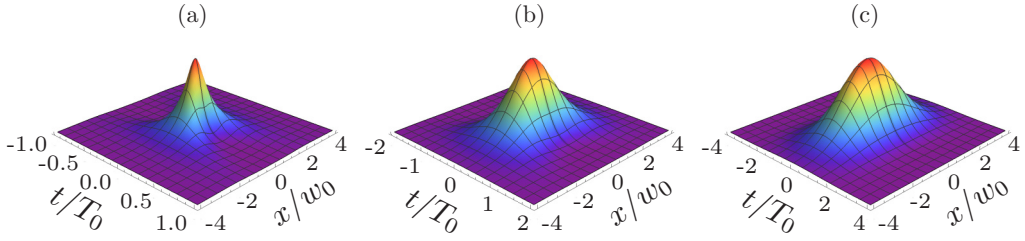

FIG. 2. Normalized spatiotemporal intensity profiles $I(x,0;t)$ for $\beta = 0.1$. (a) Subcycle pulse with $n = 1$, (b) single-cycle pulse with $n = 10$, and (c) two-cycle pulse with $n = 50$.

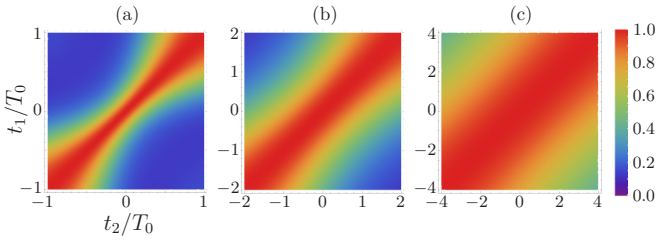

FIG. 4. Absolute value of the complex degree of temporal coherence $|\gamma(w_0,w_0,0;t_1,t_2)|$ at an off-axis spatial position $x_1 = x_2 = w_0$ and for $\beta = 0.1$. (a) Subcycle pulse with $n = 1$, (b) single-cycle pulse with $n = 10$, and (c) two-cycle pulse with $n = 50$.

Figure 4 illustrates the absolute value of the two-time complex degree of temporal coherence

$$\gamma(w_0,w_0,0;t_1,t_2) = \frac{\Gamma(w_0,w_0,0;t_1,t_2)}{\sqrt{I(w_0,0;t_1)I(w_0,0;t_2)}} \tag{55}$$

of the initial pulse at a distance $x_1 = x_2 = w_0$ from the optical axis for $\beta = 0.1$. For small values of n the temporal coherence length in the center of the pulse, i.e., for small values of the average time $\bar{t} = \frac{1}{2}(t_1 + t_2)$, is less than the pulse duration, and the temporal coherence function is not of the Schell-model form. With increasing n the width of $|\gamma(w_0,w_0,0;t_1,t_2)|$ in the antidiagonal direction becomes nearly constant (the field is temporally of the Schell-model form), and the effective coherence time rapidly becomes larger than the pulse duration.

The overall degree of temporal coherence of the train as a function of spatial position can be conveniently characterized by the quantity $\bar{\gamma}(x,z)$, defined as

$$[\bar{\gamma}(x,z)]^2 = \frac{\iint_{-\infty}^{\infty} I(x,z;t_1)I(x,z;t_2)|\gamma(x,x,z,t_1,t_2)|^2 dt_1 dt_2}{\iint_{-\infty}^{\infty} I(x,z;t_1)I(x,z;t_2) dt_1 dt_2}, \tag{56}$$

which is an intensity weighted average over the two-time degree of temporal coherence. Figure 5 illustrates this quantity for pulses with different bandwidths at $z = 0$. For subcycle pulses in particular, this effective degree of temporal coherence reduces substantially below unity within the effective spatial area of the beam.

The physical origin of the spatiotemporal coherence coupling effects can be traced to the frequency dependence of the modal scale. In view of Eq. (2), low-frequency components have a larger spatial extent than high-frequency components, and hence the spectral beam profile becomes "redshifted," when one moves away from the optical axis. This implies that the number of frequency components that effectively contribute to the beam reduces with x. This is in accordance with some previous studies on pulsed [25] and stationary [26] propagation-invariant fields, where spatial and temporal coherence are also intimately linked.

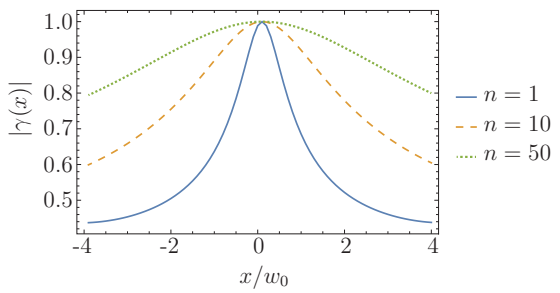

FIG. 5. Overall degree of temporal coherence scanned over the x axis for $n = 1$, $n = 10$, and $n = 50$.

Because of the isodiffractive nature of the laser resonator modes, effects similar to those shown in Figs. 3–5 are observed also at finite propagation distances. If we had assumed a frequency-independent modal scale at the waist instead of Eq. (2), the initial field at $z = 0$ would have been temporally fully coherent. However, the beam would become temporally partially coherent upon propagation because different frequency components would diverge at different rates.

VI. CONCLUSIONS

We have extended the standard concept of (stationary) Gaussian Schell-model beams into the domain of pulsed beams, using a modal representation that is consistent with the theory of multimode spherical-mirror laser resonators. Our model permits the analysis of spatiotemporal properties of ultrashort pulses of any duration, from few-cycle down to subcycle regimes. It reveals strong spatiotemporal coupling effects, which depend on the state of spatial coherence of the beam.

Given the widespread use of the Gaussian Schell model in coherence theory of stationary fields, we expect our model to find extensive use in studies of ultashort spatially partially coherent pulses and their applications. In this work full spectral coherence of the field was assumed. It appears possible to lift this restriction and allow also partial correlations between the spectral field components, but this requires further investigation.

ACKNOWLEDGMENTS

The work was financially supported by National Natural Science Foundation of China (61575091, 61675094), Education Department of Henan Province (17A140001), and Strategic funding of the University of Eastern Finland (930350).

APPENDIX A

In this Appendix we derive the final solution for the spatiotemporal field, Eqs. (44)–(48) of the main text.

Inserting from Eq. (43) into Eq. (42) and changing variables as $\sqrt{\omega_2/\omega_0} = \xi$ yields

$$J(x_1,x_2,z;t_1,t_2,\omega_1) = \frac{2(2n)^n\omega_0}{\sqrt{\Gamma(2n)}} \int_0^{\infty} \xi^{2n+1} \exp\{-[T(x_2,z;t_2)+n]\xi^2\} \times \exp\left[\frac{x_1x_2}{\sigma^2(z)}\sqrt{\frac{\omega_1}{\omega_0}}\,\xi\right] d\xi. \tag{A1}$$

The integral in this expression can be evaluated with

$$\int_0^\infty \xi^{2n+1}\exp\left(-a\xi^2+b\xi\right)d\xi = \frac{1}{2a^{n+3/2}}\left[\sqrt{a}\,\Gamma(n+1)\,{}_1F_1\left(n+1;\frac{1}{2};\frac{b^2}{4a}\right)+b\,\Gamma\left(n+\frac{3}{2}\right){}_1F_1\left(n+\frac{3}{2};\frac{3}{2};\frac{b^2}{4a}\right)\right], \tag{A2}$$

where ${}_1F_1(a;b;z)$ is the Kummer confluent hypergeometric function. Hence we get

$$\begin{aligned} J(x_1,x_2,z;t_1,t_2,\omega_1) = \frac{(2n)^n\omega_0}{\sqrt{\Gamma(2n)}}\Bigg(&\frac{\Gamma(n+1)}{[T(x_2,z;t_2)+n]^{n+1}}\,{}_1F_1\left\{n+1;\frac{1}{2};\frac{x_1^2x_2^2}{4\sigma^4(z)[T(x_2,z;t_2)+n]}\frac{\omega_1}{\omega_0}\right\}\\ &+\frac{\Gamma(n+3/2)}{[T(x_2,z;t_2)+n]^{n+3/2}}\frac{x_1x_2}{\sigma^2(z)}\sqrt{\frac{\omega_1}{\omega_0}}\,{}_1F_1\left\{n+\frac{3}{2};\frac{3}{2};\frac{x_1^2x_2^2}{4\sigma^4(z)[T(x_2,z;t_2)+n]}\frac{\omega_1}{\omega_0}\right\}\Bigg). \end{aligned} \tag{A3}$$

Inserting this expression into Eq. (40) and changing variables as $\sqrt{\omega_1/\omega_0}=\zeta$ we arrive at

$$\begin{aligned} \Gamma(x_1,x_2,z;t_1,t_2) = \frac{2(2n)^{2n}\omega_0^2}{\Gamma(2n)}\frac{w}{w(z)}\int_0^\infty \zeta^{2n+1}\exp\{-[T^*(x_1,z;t_1)+n]\zeta^2\}\\ \times\Bigg(\frac{\Gamma(n+1)}{[T(x_2,z;t_2)+n]^{n+1}}\,{}_1F_1\left\{n+1;\frac{1}{2};\frac{x_1^2x_2^2}{4\sigma^4(z)[T(x_2,z;t_2)+n]}\zeta^2\right\}\\ +\frac{\Gamma(n+3/2)}{[T(x_2,z;t_2)+n]^{n+3/2}}\frac{x_1x_2}{\sigma^2(z)}\zeta\,{}_1F_1\left\{n+\frac{3}{2};\frac{3}{2};\frac{x_1^2x_2^2}{4\sigma^4(z)[T(x_2,z;t_2)+n]}\zeta^2\right\}\Bigg)d\zeta. \end{aligned} \tag{A4}$$

The remaining integral can be evaluated with

$$\int_0^\infty \zeta^{2n+1}\exp\left(-a\zeta^2\right){}_1F_1\left(n+1;\frac{1}{2};b\zeta^2\right)d\zeta = \frac{\Gamma(n+1)}{2a^{n+1}}\,{}_2F_1\left(n+1,n+1;\frac{1}{2};\frac{b}{a}\right) \tag{A5}$$

and

$$\begin{aligned} \int_0^\infty \zeta^{2n+2}\exp\left(-a\zeta^2\right){}_1F_1\left(n+\frac{3}{2};\frac{3}{2};b\zeta^2\right)d\zeta = \frac{\Gamma(n+3/2)}{8ba^{n+3/2}(n+1)^2}\Bigg\{&(b-a)\,{}_2F_1\left(n+\frac{3}{2},n+\frac{3}{2};-\frac{1}{2};\frac{b}{a}\right)\\ &+[a-2b(2n+3)]\,{}_2F_1\left(n+\frac{3}{2};n+\frac{3}{2};\frac{1}{2};\frac{b}{a}\right)\Bigg\}, \end{aligned} \tag{A6}$$

where ${}_2F_1(a,b;c;z)$ is the Gauss hypergeometric function. The final result expressed in Eqs. (44)–(48) follows after some simplification.

APPENDIX B

In this Appendix we consider numerical issues related to the evaluation of spatiotemporal fields with large values of n. The implication is that the model considered here is numerically most appropriate for ultrashort pulses in subcycle or (at most) few-cycle regimes. This, however, is the regime we are most interested in.

The Gauss hypergeometric function can be defined for $|z|<1$ using the infinite sum

$${}_2F_1(a,b;c;z) = \sum_{m=0}^{\infty}\frac{(a)_m(b)_m}{(c)_m}\frac{z^m}{m!}, \tag{B1}$$

where $(\,)_m$ denotes the Pochhammer symbol. For large values of n the first term of the MCF is most significant and $\Gamma(x_1,x_2,z;t_1,t_2)\approx\Gamma_1(x_1,x_2,z;t_1,t_2)$. Explicitly,

$$\begin{aligned} {}_2F_1\left[n+1,n+1;\frac{1}{2};\frac{x_1^2x_2^2}{4\sigma^4(z)T_n(x_1,x_2,z;t_1,t_2)}\right] &= \sum_{m=0}^{\infty}\frac{(n+1)_m^2}{m!(\frac{1}{2})_m}\left[\frac{x_1^2x_2^2}{4\sigma^4(z)T_n(x_1,x_2,z;t_1,t_2)}\right]^m\\ &= \frac{\sqrt{\pi}}{(n!)^2}\sum_{m=0}^{\infty}\frac{(n+m)!}{m!(m-\frac{1}{2})!}\left[\frac{x_1^2x_2^2}{4\sigma^4(z)T_n(x_1,x_2,z;t_1,t_2)}\right]^m, \end{aligned} \tag{B2}$$

where the Pochhammer symbols were written in terms of factorials to get the final equality. To get numerical results with negligible error, one needs to evaluate the sum over $m\gg n$. If, e.g., $n=10$ and we evaluate the sum in the interval $x=[-4w_0,4w_0]$ for $\beta=0.1$, the numerical values of the term $m=n$ range over ~100 orders of magnitude within the area of the pulse. Hence, for

large values of n, numerical instabilities are encountered (in particular for small values of β) in the evaluation of the higher-order terms even though the MCF is mathematically well defined for any n.

[1] P. Milonni and J. H. Eberly, *Lasers* (Wiley, New York, 1988), Sects. 14.7 and 14.8.

[2] V. V. Kozlov, N. N. Rosanov, and S. Wabnitz, Obtaining single-cycle pulses from a mode-locked laser, Phys. Rev. A **84**, 053810 (2011).

[3] V. V. Kozlov and N. N. Rosanov, Single-cycle-pulse passively-mode-locked laser with inhomogeneously broadened active medium, Phys. Rev. A **87**, 043836 (2013).

[4] R. M. Arkhipov, M. V. Arkhipov, I. Babushkin, and N. N. Rosanov, Self-induced transparency mode locking, and area theorem, Opt. Lett. **41**, 737 (2016).

[5] R. W. Ziolkowski and J. B. Judkins, Propagation characteristics of ultrawide-bandwidth pulsed Gaussian beams, J. Opt. Soc. Am. A **9**, 2021 (1992).

[6] M. A. Porras, Ultrashort pulsed Gaussian light beams, Phys. Rev. E **58**, 1086 (1998).

[7] S. M. Feng, H. G. Winful, and R. W. Hellwarth, Spatiotemporal evolution of focused single-cycle electromagnetic pulses, Phys. Rev. E **59**, 4630 (1999).

[8] E. Wolf and G. S. Agarwal, Coherence theory of laser resonator modes, J. Opt. Soc. Am. A **1**, 541 (1984).

[9] L. Mandel and E. Wolf, *Optical Coherence and Quantum Optics* (Cambridge University Press, Cambridge, 1995), Sect. 5.6.4.

[10] F. Gori, Collett-Wolf sources and multimode lasers, Opt. Commun. **34**, 301 (1980).

[11] A. Starikov and E. Wolf, Coherent-mode representation of Gaussian Schell-model sources and their radiation fields, J. Opt. Soc. Am. **72**, 923 (1982).

[12] I. P. Christov, Propagation of partially coherent light pulses, Opt. Acta **33**, 63 (1986).

[13] L. G. Wang, Q. Lin, H. Chen, and S. Y. Zhu, Propagation of partially coherent pulsed beams in the spatiotemporal domain, Phys. Rev. E **67**, 056613 (2003).

[14] H. Lajunen, J. Tervo, and P. Vahimaa, Theory of spatially and spectrally partially coherent pulses, J. Opt. Soc. Am. A **22**, 1536 (2005).

[15] C. Ding, L. Pan, and B. Lü, Characterization of stochastic spatially and spectrally partially coherent electromagnetic pulsed beams, New J. Phys. **11**, 083001 (2009).

[16] C. Ding, L. Pan, and B. Lü, Changes in the spectral degree of polarization of stochastic spatially and spectrally partially coherent electromagnetic pulses in dispersive media, J. Opt. Soc. Am. B **26**, 1728 (2009).

[17] C. Chen, H. Yang, Y. Lou, and S. Tong, Second-order statistics of Gaussian Schell-model pulsed beams propagating through atmospheric turbulence, Opt. Express **19**, 15196 (2011).

[18] T. Voipio, T. Setälä, and A. T. Friberg, Coherent-mode representation of partially polarized pulsed electromagnetic beams, J. Opt. Soc. Am. A **30**, 2433 (2013).

[19] L. Sereda, M. Bertolotti, and A. Ferrari, Coherence properties of nonstationary light wave fields, J. Opt. Soc. Am. A **15**, 695 (1998).

[20] I. A. Walmsley and C. Dorrer, Characterization of ultrashort electromagnetic pulses, Adv. Opt. Photonics **1**, 308 (2009).

[21] E. Shchepakina and O. Korotkova, Spectral Gaussian Schell-model beams, Opt. Lett. **38**, 2233 (2013).

[22] E. Wolf, New theory of partial coherence in the space-frequency domain. Part I: Spectra and cross-spectra of steady-state sources, J. Opt. Soc. Am. **72**, 343 (1982).

[23] We follow largely the notation of J. Turunen, *Low coherence laser beams*, in *Laser Beam Propagation: Generation and Propagation of Customized Light*, edited by A. Forbes (CRC, Boca Raton, FL, 2014), Chap. 10.

[24] P. Vahimaa and J. Tervo, Unified measures for optical fields: Degree of polarization and effective degree of coherence, J. Opt. A: Pure Appl. Opt. **6**, S41 (2004).

[25] K. Saastamoinen, J. Turunen, P. Vahimaa, and A. T. Friberg, Spectrally partially coherent propagation-invariant fields, Phys. Rev. A **80**, 053804 (2009).

[26] J. Turunen, Space-time coherence of polychromatic propagation-invariant fields, Opt. Express **16**, 20283 (2008).